Taylor & Francis
Taylor & Francis Group

 OPEN ACCESS Check for updates

Modelling multi-scale material growth and erosion under energetic atomic deposition

Andrew M. Bell ⬩ and Paul A. Mulheran ⬩

Department of Chemical and Processing Engineering, University of Strathclyde, Glasgow, UK

ABSTRACT
We study crystalline surface evolution in extreme environments, where high-energy atoms impinge on a crystalline surface to cause sputtering, growth and surface roughening. For our model system, we study the evolution of the Ni(111) surface under Ni atom bombardment, using Molecular Dynamics (MD) simulation and a Sutton-Chen force field, where the uppermost surface layers are free to move, supported by thermostatically controlled layers above a rigid template. The MD statistics of sputtering and sticking are used to aid the development of a computationally efficient kinetic Monte Carlo (KMC) code. Comparisons between the simulation surface morphologies are used to tune the KMC growth rules so that the key statistical features of the MD structures are captured by the KMC model. This model is then employed to explore the predicted behaviour over length and times scales much larger than those accessible to MD. While the MD-KMC approach is well known, this application to the complex surface growth encountered in energetic atomic bombardment illuminates the complexities of relating atomistic events to morphological evolution. The work shows how simulation methodology can be extended to provide predictive capabilities, paving the way for design tools for engineering processes such as plasma deposition film growth.

1. Introduction

The surface evolution of a material caused by energetic atomic impacts is important in a variety of different areas, such as crystal growth in plasma deposition and erosion in space vehicle re-entry [1,2]. Metals provide good model systems, since not only are they important engineering materials, there are well-established modelling approaches for them. Therefore, in this work, we will model the surface evolution of the Ni(111) surface under energetic bombardment by Ni atoms, with a view to understanding the statistical properties of its long-term evolution. This will require the application of different modelling techniques, so that atomistic detail can be used to inform structural evolution on large length and time scales much beyond the reach of atomistic simulation.

Atomistic molecular dynamics (MD) simulations have been used for a number of applications [3–12]. There are various different potential models for the atomic interactions that can be utilised in MD, such as the Lennard-Jones potential, used for simple pairwise interactions; the Tersoff potential [13], used for more complex systems where pair-potentials do not capture the physics well; and the Embedded Atom Method (EAM), typically used for metallic bonding. There are a number of variations on EAM such as the Finnis-Sinclair [14] and the Sutton-Chen potentials, which provides conveniently parameterised pair functionals for the interaction potentials [15,16]. In this work we will employ the Sutton-Chen potential, since it has been successfully used to simulate various properties of

metals and alloys [8–12], although it might be that this potential underestimates surface diffusion barrier.

Atomistic MD simulations have been used previously to model deposition and thin-film growth. Examples include the growth of an amorphous carbon film [17]; the deposition of aluminium atoms on a crystalline Al substrate [18–23]; the deposition of Cu on Cu, [24–26] and Ar on Cu [24]; and noble gases on magnesium oxide and magnesium hydroxide [27–29].

An alternative modelling approach employs Kinetic Monte Carlo as a mesoscopic simulation method, aiming to capture the main features of the atomistic growth process through a set of simplified probabilities rather than the full atomistic detail of the system's dynamics. Lattice-based KMC and off-lattice KMC have both been used for thin-film growth, with various alternative strategies. Accelerated KMC using on-the-fly saddle point searches provides one interesting alterative [30], while Kenny et al [31,32] used a hybrid MD-KMC code for simulations over long timescales. This hybrid approach illustrates the difficulty of combining MD data with higher-level methods like KMC.

In this work, we seek to develop a KMC code for simulating longer timescales using data derived from our MD simulations. We find that the complexity of the growth processes, where sputtering and surface re-organisation play crucial roles, necessitates a range of KMC growth rules that need careful tuning to capture the essential morphological features of

 Supplemental data for this article can be accessed online at https://doi.org/10.1080/08927022.2022.2097282.

the surface evolution. This extension of the MD-KMC model-ling strategy to extreme environments illuminates the wider challenges of multiscale modelling [33], and in particular how the connection between atomistic process and larger scale morphological evolution can be made in such a way that is relevant to engineering applications where energetic atomistic bombardment is inevitable.

This paper is organised as follows. The methodology is presented first for the MD simulations, which employs a shifted second-derivative cutoff with Sutton-Chen potentials for face-centred-cubic (fcc) Ni metal. An algorithm for surface identification is also presented, which provides important metrics that aid the development of the KMC simulation methodology that follows. The KMC considers deposition, sputtering and relaxation events, introducing a set of parameters that are tuned to reproduce key statistics from the MD results. The MD simulation results are presented next, followed by the KMC results optimised to the MD behaviour. The KMC is then exploited to consider extended length and time scales, along with an analysis of its scaling behaviour. The paper finishes with conclusions drawn from this multiscale modelling approach.

2. Methodology

2.1. Molecular dynamics

In this work, Molecular Dynamics simulations were performed using a code developed in-house by the authors. The code utilised the Sutton-Chen potential [15,16] and used the velocity-Verlet algorithm [34] to integrate Newton's equations of motion. The Sutton-Chen parameters used are given in Table S1 of the Supplementary Material, and are designed to

model metallic Ni [16]. A shifted second derivative cutoff was used so that the potential and the forces go smoothly to zero at a cutoff of twice the lattice parameter (a in Table S1) [35], and a modified cell index neighbour list [36,37] was used to reduce the computational cost. A more detailed explanation of the shifted second derivative cutoff, and Figure S1 showing how different cutoff methods affect the forces on an atom at the cutoff, are available in the Supplementary Material.

The simulations start with a crystalline slab with fcc structure, with periodic boundary conditions in the x- and y-directions so that the z-direction is normal to the close-packed (111) surface exposed to the impinging atoms. The crystal's dimensions are given as m×n where m is the number of atoms in the x-direction and n is the number of atoms in the y-direction. The crystal's lowest layers were fixed and a Berendsen thermostat [38] was applied to the rest of the sub-surface layers (the time constant was 100 fs and time step was 1 fs). This is done to dampen impacts to more accurately replicate a crystal that is orders of magnitude larger than the model that can feasibly be studied. During simulations, the thermostat is active for a set amount of time between impacts, referred to as the thermalisation time. Figure 1 illustrates the simulation set-up.

2.1.1. Surface identification
An algorithm was developed to characterise the crystal's surface. The algorithm counted the number of neighbouring atoms each has; an atom is neighbouring if it is within 0.9 lattice parameters. The algorithm also accounted for other atoms potentially screening the atom being checked from the surface; these are within 1.8 lattice parameters and higher (have greater z), and where the magnitude of the difference in height is greater than 90% of the magnitude of the separation. Atoms
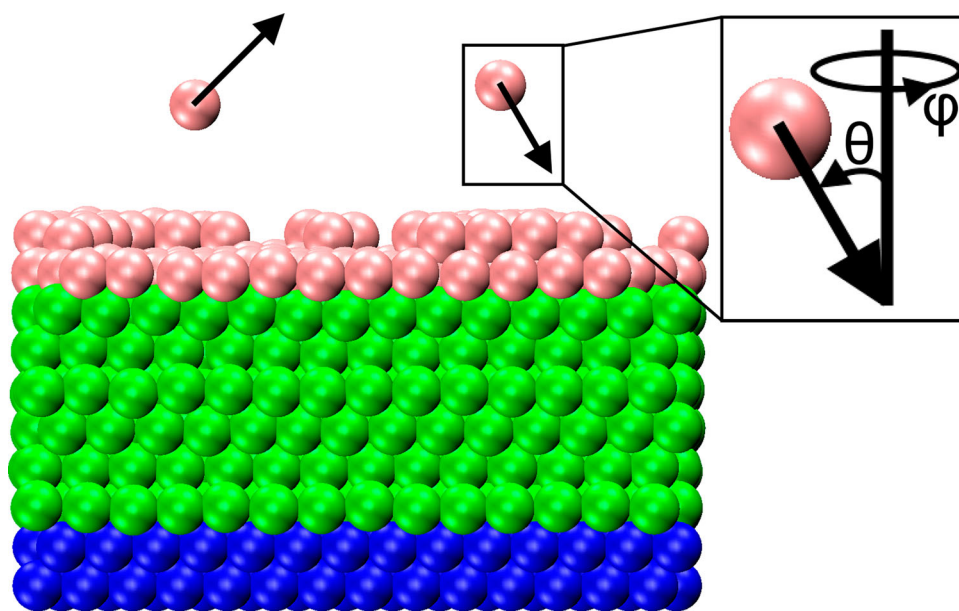

Figure 1. (Colour online) Schematic diagram of slab structure and deposition simulations. Blue atoms indicate the fixed layers while green atoms indicate the thermostatically controlled layers. Pink atoms are free-moving. The lower layer of pink atoms was the original surface layer and the higher layer is being formed by depositions. The pink atoms above the slab with black arrows are examples of a former surface atom being sputtered away on the left and an impacting atom on the right with the black arrows representing their trajectories. The inset diagram shows a representation of the polar (θ) and azimuthal (φ) angles for the impacting atom measured with respect to the surface normal.

were determined to be surface atoms if they had between 4 and 11 neighbours and were not obscured by other atoms. Once all atoms had been checked, the algorithm calculated the average surface height and the surface roughness, which we defined as the standard deviation of the surface.

To begin with, impacting atoms were given 100 eV of kinetic energy and placed 30 Å above a random point on the surface. Tests were carried out at 300 K looking at how the surface height was affected by increasing the number of impacts, increasing the surface size and altering the time between impacts as well as how long the thermostat was active. Work was also carried out to analyse the effect that the polar angle had on the behaviour of the surface at 300 K. Multiple simulations were carried out at polar angles of 10°, 20°, … 80°.

2.2. Kinetic Monte Carlo

In this work, kinetic Monte Carlo simulations were performed using an in-house code. The code uses a 2D lattice to record the surface height of an fcc crystal with a (111) surface. Using the surface height, each site in the 2D lattice is translated to the corresponding position in a (111) crystal using Equations (1–3),

$$x_{i,j} = i + \frac{1}{2}\left(\left(j - \frac{2j}{|j|}\left\lfloor\frac{|j|}{2}\right\rfloor\right) + h_{i,j}\right) \quad (1)$$

$$y_{i,j} = \frac{\sqrt{3}}{6}(3j + h_{i,j}) \quad (2)$$

$$z_{i,j} = \frac{\sqrt{3}}{2}h_{i,j} \quad (3)$$

Here $x_{i,j}$, $y_{i,j}$ and $z_{i,j}$ are the Cartesian coordinates of lattice site (i,j), i and j are the lattice indices of site (i,j) and $h_{i,j}$ is the lattice height of site (i,j). The effect of j on the x coordinate has been modified to make the output crystal surface rectangular. Lattice sites that are determined to be exposed at a step are counted again at a lower height to account for the supporting atom exposed to the surface.

2.2.1. Deposition

We add particles one by one at random sites on the lattice, with a probability that reflects the average deposition rate used in the corresponding MD simulations. Data obtained from the MD simulations are used to produce the probabilities of the particle sticking to the surface and/or causing a surface atom to be sputtered. A site on the surface is chosen using Fortran's random number intrinsic function (additional functions using Process ID and clock time generate twelve 64-bit integers at run time that are subsequently used as the seed) and if the particle is successfully deposited, the two neighbour sites that correspond to the other atoms that the deposited atom would rest upon are checked to ensure that the increase in height at the deposition site will not create an unrealistic overhang on the corresponding fcc(111) surface. If it does, one of the neighbour sites is chosen as the location where the impacting particle adheres, increasing its height instead of the original impact site. For site (i,j), the neighbour sites are identified through $(i + 1, j)$ and either $(i, j + 1)$ or $(i + 1, j + 1)$ for odd/even j.

2.2.2. Sputtering

If the particle is determined to have caused sputtering in the Monte Carlo procedure, a random site close to the initial site is selected. As in deposition, the two neighbour sites that correspond to the atoms that could rest upon the sputtered atom are checked to avoid an unrealistic overhang on the surface, and one of the neighbour sites is chosen for sputtering if necessary.

2.2.3. Relaxation

After an impact, a number of surface relaxation moves are performed, in order to replicate the atomistic processes without including all of the atomistic detail. These moves are performed by reducing the height of a chosen site by one unit, and increasing that of another selected site by the same amount. Both sites check the relevant neighbour sites, with the first checking the sputtering neighbour sites and the second checking the deposition neighbour sites. The rules that govern the probabilities of the moves, and the selection of the neighbouring sites, is motivated by the desire to replicate the statistical properties of the MD simulations but in an efficient manner that will allow the consequences of the rules to be explored on much larger systems than can be achieved with the atomistic MD simulations.

2.2.4. Production code

The production version of the kinetic Monte Carlo code was developed to allow a number of restricted surface relaxation movements after an impact, with the number of movements being set as a parameter, and more restricted surface relaxation movements occurring between impacts. The code also employed a method to try to emulate the effect of the Schwoebel barrier, which is an energy barrier that restricts atoms passing over a step to a lower layer. The probability of overcoming the Schwoebel barrier was treated as an exponential decay, in the form of

$$P = \text{Min}\left\{1, e^{-\left(\frac{nb1 + S_w - nb2}{k}\right)}\right\} \quad (4)$$

where nb1 and nb2 are the number of neighbouring atoms at the current site of an atom and the destination site, k is a constant and S_w is a parameter that treats the Schwoebel barrier as being equivalent to the barrier that must be overcome to move away from a number of neighbouring atoms. In this way, the barrier would always be overcome if the destination site had S_w more neighbouring atoms. For the simulations in this work, the S_w parameter is given values of 0, 5 and 10. The relaxing atoms selected for surface relaxation movements are restricted to being within a certain distance of the site of the previous impact, with the distance being determined by parameter D4. Some simulations allow the atom to be selected from anywhere on the surface by giving D4 a value larger than the length and width of the surface, effectively setting D4 to infinity. A visual representation of D4 and four other distance-based parameters (D1, D2, D3 and D5) is shown in Figure 2. The various parameters used in the KMC simulation are summarised in Table 1.
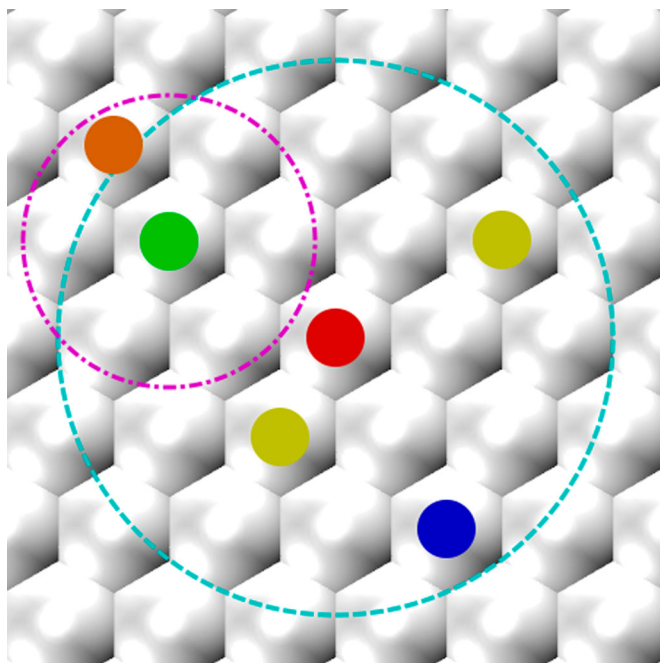
Figure 2. (Colour online) Schematic diagram of the parameters D1–D5. The atom with the red circle represents the impact site, and the cyan dotted circle represents the limits of D1, D2, D3 and D4, which are all based on the distance from the impact site. All four can have different values to each other but are shown with the same value in the figure for clarity. The atom with the blue circle, limited by D1, is the atom chosen to be sputtered. The atoms with the yellow circles, limited by D2 and D3, are the atoms chosen for surface relaxation movements after an impact. The atom with the green circle, limited by D4, is the relaxing atom selected for surface relaxation movements between impacts. The magenta dotted circle represents the limits of D5 and is based on the distance from the relaxing atom. The atom with the orange circle, limited by D5, is the site to which the relaxing atom tries to move.

Bringing these together, the model proceeds as follows:

1. A lattice site is chosen at random and a deposition takes place with a sticking probability of 0.835, which is taken from the equivalent MD simulation.
2. Similarly, a randomly chosen site within D1 of the impact site is selected to be sputtered with a probability of 0.427.
3. Two sites within D2 and D3 of the impact site are selected, their heights compared and the height of the taller (or first) site is decreased by 1 while the height of the other is increased by 1. This step is repeated N_{PI} times, representing highly energetic, disruptive post-impact events.
4. The time increment is drawn from a Poisson distribution with the rate determined by the MD deposition rate.
5. A site within D4 of the impact site and a site within D5 of the previous site are selected, their heights and number of

Table 1. Description of the parameters used in the KMC simulations.

Parameter	Explanation
D1	Maximum distance between impact site and sputtered atom
D2	Maximum distance between impact site and one post-impact relaxation site
D3	Maximum distance between impact site and the other post-impact relaxation site
D4	Maximum distance between impact site and relaxation site
D5	Maximum distance between relaxation site and destination site
S_w	The number of atoms that are treated as having an energy barrier equal in strength to the Schwoebel barrier
N_{PI}	Number of less restricted relaxation events that occur post-impact

neighbours compared and if the first site is not lower than the second the probability of the height of the first site decreasing by 1 and the second increasing by 1 is determined by Equation (4). This step is repeated by the factor that the time increment is larger than 1 fs, allowing for thermalised diffusion events between impacts.

Note that the results obtained from this model do not depend on the Sutton Chen parameters.

3. Results

3.1. Molecular dynamics

In Figure 3, the 28 × 14 surface with 4 ps thermalisation time is shown at the beginning of the simulation and in intervals of 0.51 monolayers (ML) deposited (200 atomic impacts) up to 2.55 ML deposited (1000 atomic impacts). The impacting atoms each had a polar angle of 10° and a random azimuthal angle. The formation of islands and large vacancies can be seen after the first 0.51 ML are deposited. These islands continue to grow forming almost complete layers on top of the initial surface while the number of vacancies decreases as more monolayers are deposited. The methodology cannot capture slow thermal diffusive events that might occur over longer timescales between impacts, but these are expected to be rare for the 300 K temperature used in the simulations.

Simulations were performed on a number of surface sizes and thermalisation times at 300 K to determine reliable parameters for subsequent work. The evolution of the average surface height for various simulations is displayed in Figure 4(a).

For the simulations that used 0.6 ps of thermalisation time, it was observed that the simulations had finite size effects. This can be observed from comparing the rate of growth of the simulations with the 14 × 14 surface, the 28 × 14 surface and the 28 × 28 surface using 0.6 ps. The 14 × 14 surface has a sudden surge of growth while the 28 × 14 grows steadily and the 28 × 28 contracts slightly before growing steadily. These simulations were therefore physically unrealistic for smaller surfaces. The finite size effects were not observed in simulations that had longer thermalisation times; all simulations using 4 ps of thermalisation time had similar growth rates.

The simulations using 4 ps of thermalisation time appear to have a surface height decrease for a brief period at the beginning of deposition before growing as expected. This is most likely caused by the roughening of the surface, causing the large vacancies like those in Figure 3(b) to appear. Each vacancy will cause at least the atom below the initial surface to be exposed and become a surface atom but as the surface roughens initially, two or three atoms are exposed, amplifying the effect of a surface atom sputtering on the average surface height. It was also noted that the 28 × 28 surface simulated at 0.6 ps of thermalisation time produced growth rates that are similar to those seen for the simulations at longer thermalisation times, suggesting that the finite size effects are almost eliminated at that surface size.

When analysing the surface roughness (defined earlier as the standard deviation of the surface) in Figure 4(b), it was observed that the surface in all simulations rapidly roughens
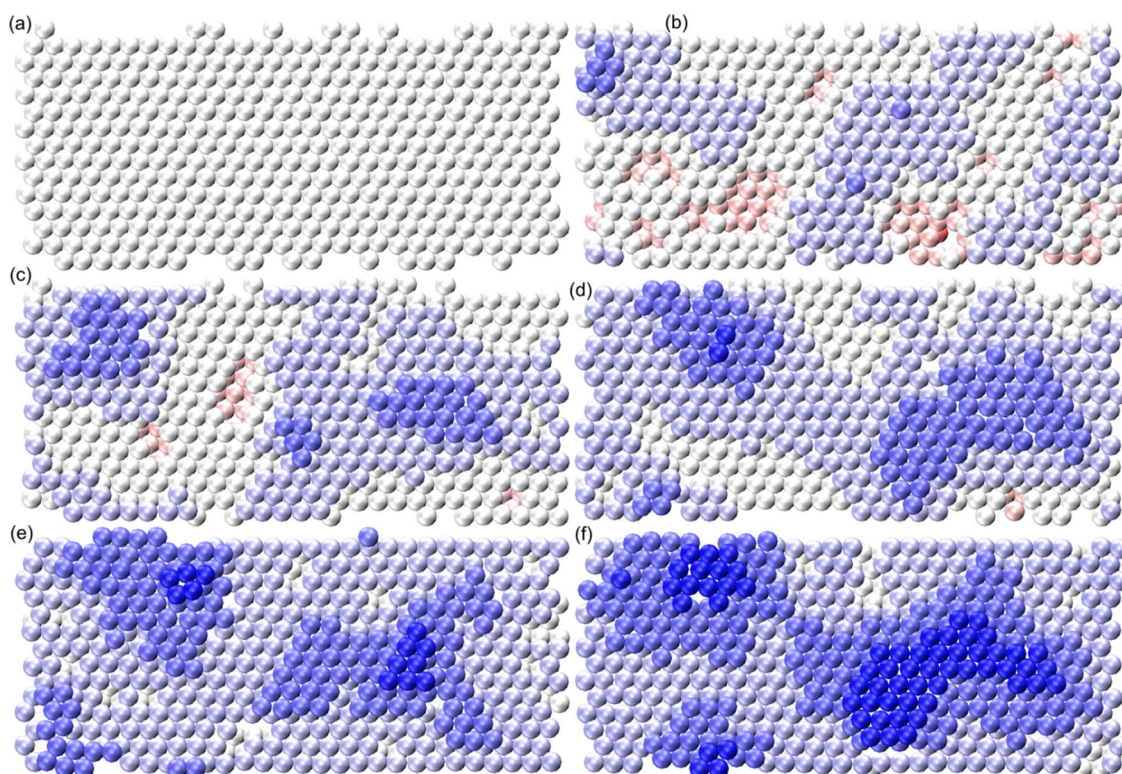
Figure 3. (Colour online) The 28 × 14 surface after (a) 0 impacts, (b) 200 impacts, (c) 400 impacts, (d) 600 impacts, (e) 800 impacts and (f) 1000 impacts. A colour gradient is being used to represent surface height with white being the height of the initial surface layer, blue being above the initial height and red being below the initial height.

initially before gradually plateauing off. Indeed, it was found that the surface roughens faster even than a power law (data not shown) until it begins plateauing. The most rapid roughening occurs at the same time as the surface appears to briefly decrease in height. It can be noted that the surface roughness can change drastically for a prolonged period. This can be seen between 1.75 and 2.25 ML deposited for the simulation with 1000 impacts on a 28 × 14 surface, where the roughness dips by approximately 0.25 Å before returning to values seen prior to 1.75 ML deposited. For the 14 × 14 surface, short thermalisation times caused the surface roughness to fluctuate wildly, which is likely due to the finite size effects noted earlier.

From these observations, a thermalisation time of 4 ps was selected to be used in subsequent simulations. The simulation shown in Figure 3 is an example of this. Simulations were then run to analyse how the polar angle of the impacting atoms affected the surface's evolution over time.

In Figure 5(a), the effect of the impacting atom's polar angle on the average surface height is analysed. In each case, the azimuthal angle is randomly selected for each impinging atom. Surface growth is observed when using a polar angle of 10°, 20°, 30° or 40°. The rate of surface growth declines as the polar angle increases. Meanwhile, surface erosion is observed with polar angles of 50°, 60°, 70° and 80°. The rate of surface erosion increased between 50° and 60° but then declined as the polar angle increased further. The decline is caused by decreasing damage caused to the surface by the impacting atom, as it is less likely the impacting atom will stick to the surface at higher polar angles (the sticking probability and sputter

yield as a function of angle of incidence are reported elsewhere [39]). It is also noted that the rapid decrease in surface height that appears to happen after the initial impacts at 10°, 20° and 30° is less prominent at 60° and is not observed at 70° and 80°. This is likely due to the lower levels of interaction, which would cause the surface to roughen more gradually than at the lower polar angles.

The effect of the polar and azimuthal angles on the surface roughness was examined in Figure 5(b). Surface roughness grew in all cases. There was a negligible difference in the surface roughness between polar angles of 10° and 30°, which can be seen as the 10°, 20° and 30° simulations all reach a surface roughness of 0.7 h_{ML}, where h_{ML} is the height of one monolayer. At 60°, there is a slight decrease in the surface roughness. More substantial decreases are observed for 70° and 80°, with under 0.5 h_{ML} of surface roughness at 70° and roughly 0.3 h_{ML} at 80°. This is due the fact that impinging atoms at these angles are more likely to be deflected after hitting the surface, maintaining most of their momentum.

3.2. Kinetic Monte Carlo

As described above, the KMC simulation has a large number of parameters (see Table 1 and Figure 2 for explanation of these), capturing a range of surface rearrangements following deposition. We have found that all of these processes are necessary to capture the morphological evolution of the surface. To determine suitable values of these parameters, a wide range of simulations have been performed. The resulting surfaces
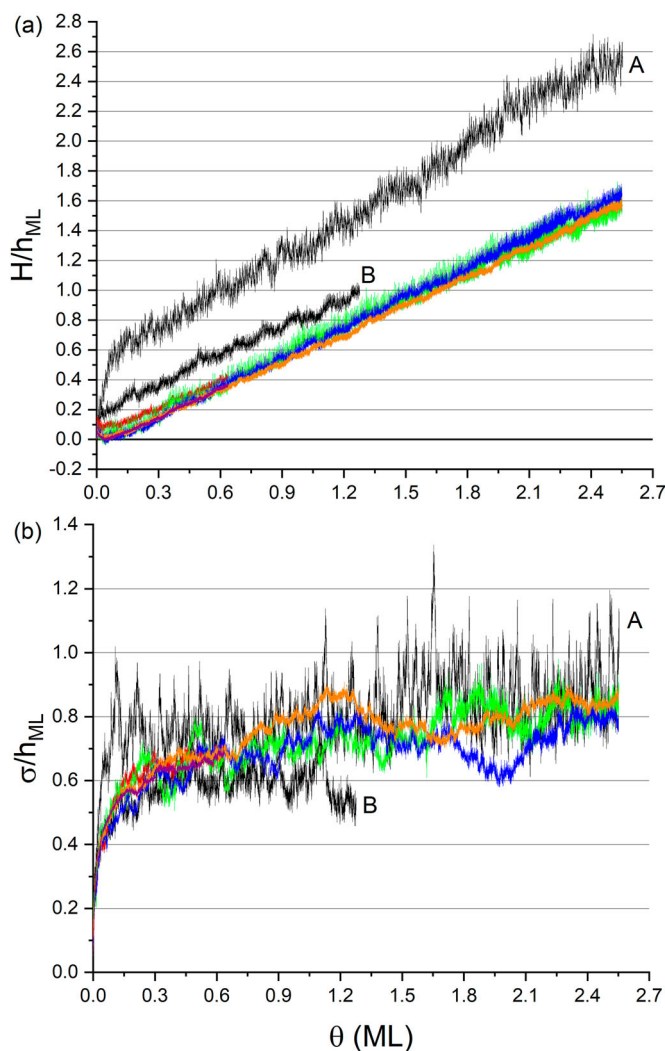
Figure 4. (Colour online) Comparison of surface statistics using different therma-lisation times and surface sizes. Three of the simulations use 0.6 ps thermalisation time and have 500 impacts on a 14 × 14 surface (black line marked A), on a 28 × 14 surface (black line marked B) and on a 28 × 28 surface (red line). The other four simulations use 4 ps thermalisation time and have 500 impacts on a 14 × 14 surface (green line), 1000 impacts on a 28 × 14 surface (blue line), 2000 impacts on a 28 × 28 surface (orange line) and 1000 impacts on a 56 × 28 surface (purple line). (a) shows average surface height (H) against ML deposited (θ) while (b) shows surface roughness (σ) against ML deposited. Values for surface height and surface roughness are normalised against the height of a monolayer (hML).

Figure 5. (Colour online) Comparison of surface statistics using different polar angles with 1000 impacts on the 56 × 28 surface. The black lines marked A, B, C and D are 10°, 20°, 30° and 40°, respectively. These four represent the cases where surface growth was seen, while 50° (red line), 60° (green line), 70° (blue line) and 80° (orange line) are the four cases in which surface erosion was seen. (a) shows average surface height (H) against ML deposited (θ) while (b) shows surface roughness (σ) against ML deposited. The lines for B and C are not shown in (b) as they are indistinguishable from A and D.

from nine different simulations are shown in Figure 6, with the parameter values employed reported in Table 2.

It is clear that the KMC is capable of producing a range of surface morphologies. Comparing to the MD results shown in Figure 3, it is apparent that images (a), (d) and (g) in Figure 6 are smoother than required. These all have zero Schwoebel barrier, confirming that it must be included in the KMC to recreate the MD growth morphologies. This is no surprise, since the impact of this transport barrier is well known [33]. Similarly, images (c), (f) and (i) in Figure 6 are also smoother than required. These all have large values of the parameter D4, which sets the range of the surface relaxation events (see Table 1).

Consequently, we will focus now on the simulations (b), (e) and (h) for Figure 6, and for simplicity refer to these as cases 1, 2 and 3 respectively. These all have non-zero Schwoebel barrier, but with different strengths, and local relaxations
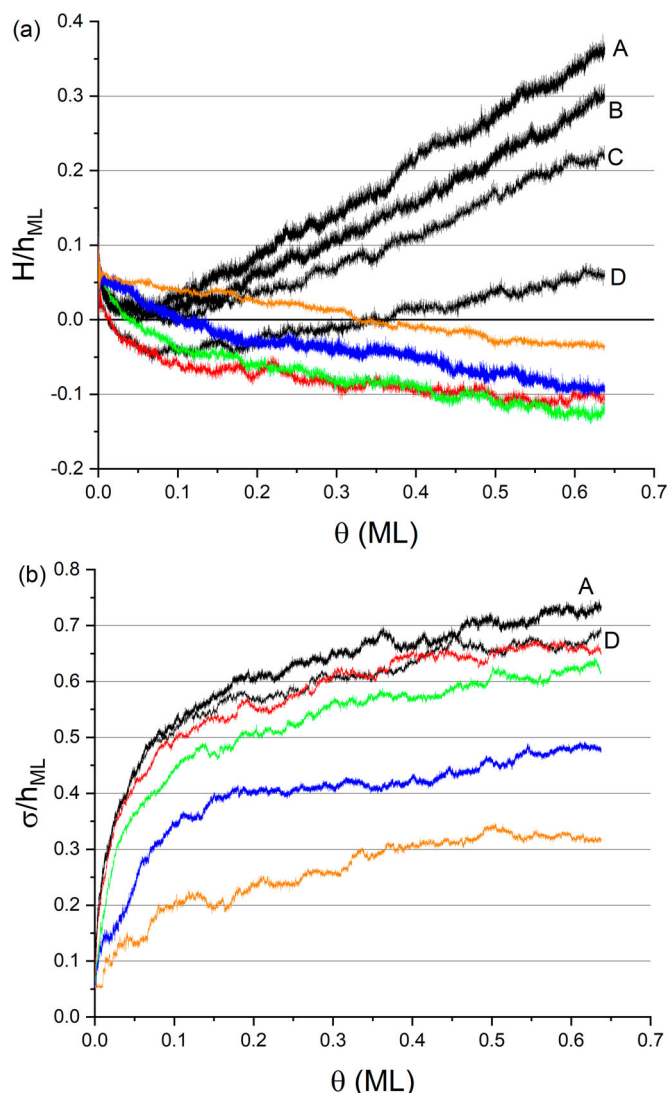
following deposition mixed with differing numbers of unrestricted relaxations determined by N_{PI} (see Table 1).

Cases 1, 2 and 3 were re-run multiple times to obtain averages of 15 runs. These averages are compared to the average of three MD runs in Figure 7. It can be seen in Figure 7(a) that the underlying trends of the average surface height in Cases 2 and 3 both match the trend seen in the MD very well, with both producing a very similar initial decrease in the surface height. Meanwhile, Case 1 had a much more limited decrease in the average surface height. When the average surface height began to grow linearly, all simulations followed a similar trend.

From Figure 7(b), it can be seen that underlying trend of the surface roughness in Case 1 is very close to the surface roughness observed in the MD during the rapid roughening phase at the beginning but as the simulation progresses the MD
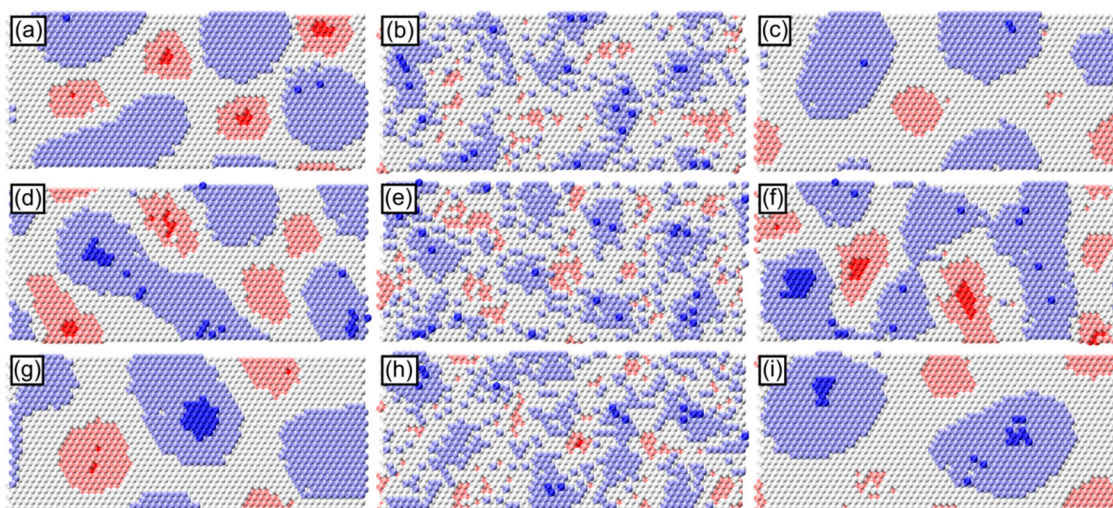
Figure 6. (Colour online) Comparison of nine surfaces produced using the KMC code after 1000 deposition events on 28 by 14 surfaces. Each surface shown uses a colour gradient to denote height with blue denoting higher atoms, red denoting lower atoms and white denoting the midpoint of the heights.

roughens faster than Case 1. The underlying trends of the surface roughness in Cases 2 and 3 show that these simulations tend to roughen faster than the MD throughout the simulation. Beyond the duration of the MD simulation, the surface roughness in the three KMC simulations begin to converge. By the end of the KMC simulations, Cases 1 and 2 are likely to have converged while the surface in Case 3 tends to be slightly rougher. Recall from Table 2 that Case 3 uses a Schwoebel barrier that is treated as equivalent in energy to 10 neighbour atoms instead of the 5 atoms used in Cases 1 and 2. This increase may be restricting the filling of vacancies which could be causing the surface to be slightly rougher than Cases 1 and 2. The slower surface roughening at the beginning of the simulation in Case 1 compared to Cases 2 and 3 is likely caused by Case 1 only having two impact movements instead of five like Cases 2 and 3 (see Table 3). These movements can cause the formation of vacancies and islands so the decreased amount of impact movements means islands and vacancies are formed slower leading to slower surface roughening.

3.2.1. Surface growth analysis
From the above figures, we determined that the simulation conditions in Case 2 are most likely the best compromise. Case 2 produced a reasonably good match with the MD when looking at average surface height but had a poorer match when considering surface roughness.

A comparison of the MD and the KMC is shown in Figure 8. It can be seen that the KMC produces a rough approximation of the MD with adatom islands and vacancies spread across the surface but with the KMC islands being more disjointed. This is also the case for the initial atoms forming a second island layer with the KMC having almost no connected atoms while the MD has formed a number of compact 2nd-layer islands.

In Figure 9, we look at the surface roughness throughout the deposition of the equivalent of 40 ML on surfaces starting with the initial 56×28 used for KMC and doubling the surface in alternating dimensions to 56×56, 112×56, 112×112 and 224×112. Compared to the larger simulations, the 56×28 surface appears to roughen quicker until it reaches the equivalent of 20 ML deposited when it levels off at a surface roughness equivalent to the height of 1.2 ML. The larger systems on the other hand, continue to roughen for the duration of the deposition. From this, it is clear that the 56×28 surface is not suitable for deposition simulations longer than 20 ML as it will suffer from finite size effects. However, it is very likely that the 56×28 surface suffers from finite size effects much earlier than this as the comparison of repeated runs with the 56×28 surface (not shown) reveal differences in the surface roughness of up to 0.15 as early as the equivalent of five monolayers deposited.

In the inset of Figure 9, we plot the log of the surface roughness against the log of the ML deposited. The data shown begins from the equivalent of ~0.2 ML deposited as the data below 0.2 ML is sparse but would contribute to a large proportion of the plot, which means it would fluctuate rapidly and drastically skew any trend lines. Linear trend lines were fit to the logarithm of the surface roughness for each of the simulations. The gradients of the trend lines are detailed in Table 3. All of the trend line gradients have a confidence interval taken from the standard deviation of gradients from trend lines fit to random subsets of the data.

The trend line gradient for the 56×28 surface is much lower than the other gradients. This is because the surface roughness levelled off, ending the apparent power law growth seen earlier in the simulation. It is interesting to note that the gradients for the larger systems are much lower than ½ [40]

Table 2. Parameter values used in the nine simulations are shown in Figure 7.

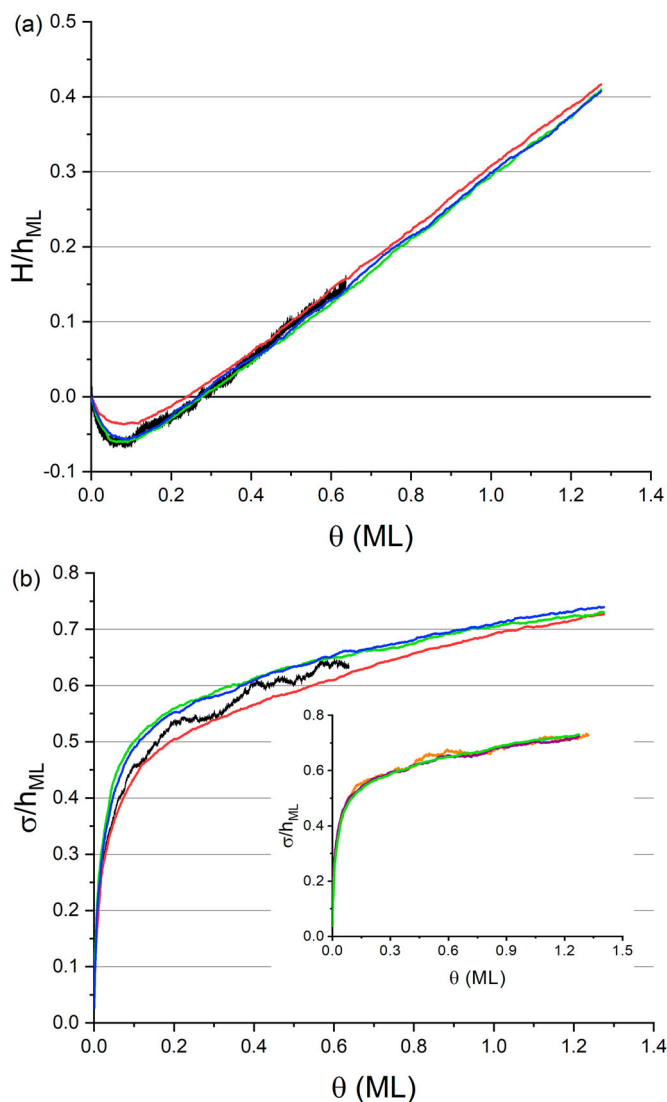| Run	S_w	N_{PI}	D1	D2	D3	D4	D5
(a)	0	2	4	4	4	∞	2
(b): Case 1	5	2	4	4	4	1	2
(c)	5	2	4	4	4	∞	4
(d)	0	5	4	4	4	∞	2
(e): Case 2	5	5	4	4	4	1	2
(f)	5	5	4	4	4	6	1
(g)	0	5	4	4	4	∞	4
(h): Case 3	10	5	4	4	4	1	2
(i)	10	5	4	4	4	6	4

Figure 7. (Colour online) Comparison of surface statistics between the molecular dynamics and the kinetic Monte Carlo simulations. The black line is the average of three simulations performed with the MD. The three candidate cases of the KMC are averaged over 15 simulations with Case 1 shown in red, Case 2 shown in green and Case 3 shown in blue. (a) shows average surface height (H) against ML deposited (θ) while (b) shows surface roughness (σ) against ML deposited. The inset graph in (b) shows the effects of noise on Case 2 of the KMC with the results of a single simulation (orange line), the average of three simulations (purple line) and the average of 15 simulations (green line).

due to the various surface relaxation events occurring in the simulations.

Looking back at the inset of Figure 9, the trend line fit through the 224×112 surface data (the purple line in Figure 10) matches the data well after $\log(\theta) \sim 0.4$ (2.5 ML) but prior to that point, the surface appears to grow more slowly.

Table 3. The gradient of the trend line fit to each simulation in the inset of Figure 10.

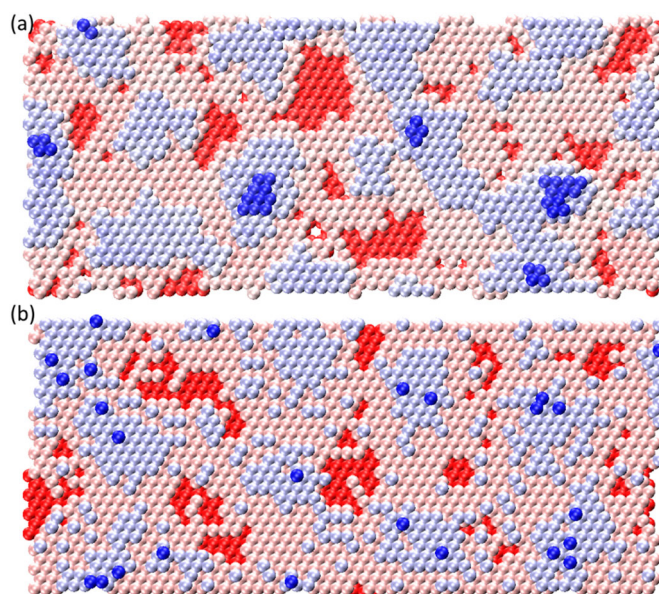| Surface size	Trend line gradient
56×28	0.141 ± 0.005
56×56	0.185 ± 0.005
112×56	0.167 ± 0.003
112×112	0.168 ± 0.003
224×112	0.171 ± 0.002

Figure 8. (Colour online) Comparison of the surface from an MD simulation (a) to a Case 2 KMC simulation (b) after 1000 deposition events on 28 by 14 surfaces. Both surfaces use the same colour gradient for height with blue denoting higher atoms, red denoting lower atoms, and, for these simulations, pink denoting the initial surface height.

It should be noted that this is roughly the point where the average surface height reaches the equivalent of 1 ML. This would imply that while the rate of surface growth remains roughly constant around that point, the dynamics of the surface growth changes as the surface approaches the equivalent of one ML added, causing the surface to roughen more quickly as it grows further.

In Figure 10, we look at the surfaces obtained at the end of the simulations analysed in Figure 9, produced by running
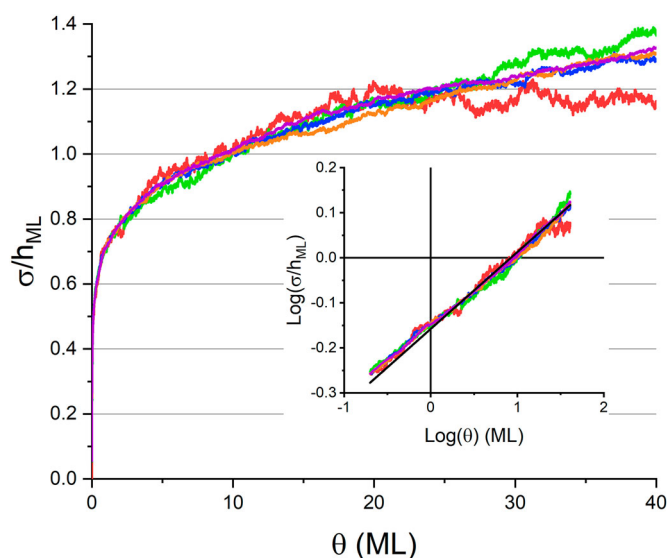

Figure 9. (Colour online) Comparison of surface roughness (σ) against ML deposited (θ) at various surface sizes for the KMC. Each surface was impacted by the equivalent of 40 ML. The surfaces simulated were 56×28 (red), 56×56 (green), 112×56 (blue), 112×112 (orange) and 224×112 (purple). The inset graph plots the logarithm of the surface roughness against the logarithm of the ML deposited. A linear fit (black line) was also plotted.
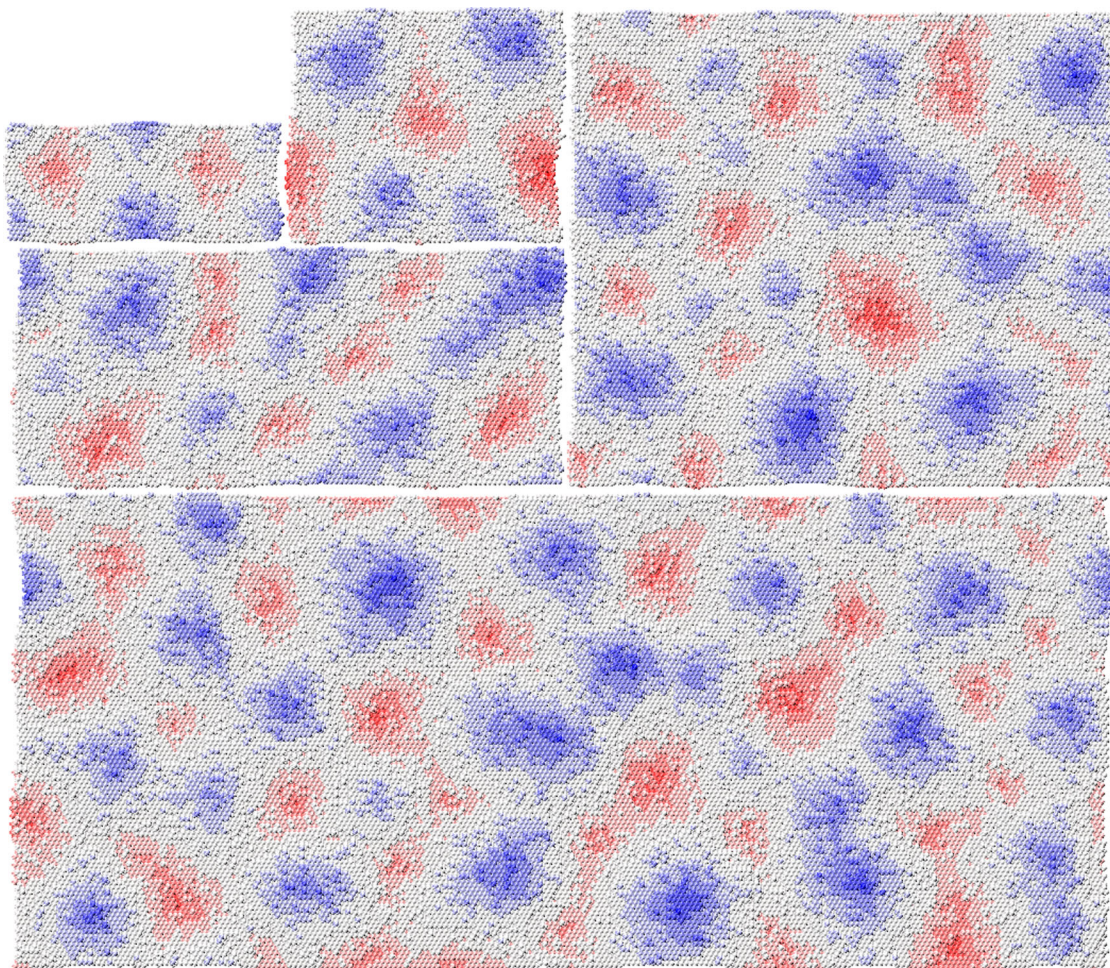
Figure 10. (Colour online) The final surface of Case 2 KMC simulations after deposition of 40 ML at surface sizes 56 × 28, 56 × 56, 112 × 56, 112 × 112 and 224 × 112, displayed to scale.

Case 2 KMC simulations until the equivalent of 40 ML have been deposited. Comparing the 224 × 112 surface to the 56 × 28 surface, it is clear that, as concluded in Figure 9, the 56 × 28 surface is being heavily affected by finite size effects with very shallow vacancies and relatively small islands packed closer together than the islands and vacancies on the 224 × 112 surface. However, when comparing the 224 × 112 surface to the rest of the surfaces, it appears the 56 × 56 and 112 × 56 surfaces may also be affected by finite size effects, with the 56 × 56 surface appearing to have its islands and vacancies more ordered than the 224 × 112 and 112 × 112 surfaces. The 112 × 56 surface also appears to be more ordered, but only in the y-direction (up the page). This could suggest that a slab used to simulate the evolution of the surface over the deposition of the equivalent of 40 ML must be larger than 56 lattice sites in both directions. The 112 × 112 surface appears to be unaffected by finite size effects so, of the five surfaces used, this represents the minimum surface size that can simulate the deposition of the equivalent of 40 ML without being affected by finite size effects.

We conclude that finite size effects constrain the minimum surface size required to accurately simulate deposition and the minimum required size is proportional to how much deposition occurs. This means that as larger amounts of deposition is required, so too are larger surfaces, as seen in Figure 9, where

the 56 × 28 surface was shown to be unsuitable for simulations greater than 20 ML. This will cause the computational load to grow nonlinearly ($\sim N^3$) with increasing number N of deposited ML.

Considering that with the constraints on processing power, a 40 ML deposition on a 14 by 14 surface took in the order of weeks using MD and that it was later determined that a 112 by 112 was the minimum size that could reliably simulate 40 ML deposition without finite size effects, it is clear that a MD simulation without finite size effects for the deposition of the equivalent of 40 ML is very computationally expensive to run, as it would have to run for several decades with the practical computational constraints we deal with. However, the same simulation in KMC only took approximately an hour on a single core of an Intel Xeon E5420 @ 2.5 GHz, compared to the 12 cores of Intel Xeon X5650 @ 2.66 GHz used for the MD simulation, so the speed-up is of the order of 5000.

4. Summary and conclusions

Simulations of the growth of a material surface under energetic atomic bombardment have been presented using both MD and KMC, with the latter requiring the inclusion of a range of growth processes and concomitant parameter tuning to replicate the MD results. Nevertheless, the KMC provides the

flexibility to investigate finite size effects, overcoming the serious limitations of MD that restrict exploration of scaling effects.

We have used the growth of a Ni(111) surface as our model system. Our MD results show the balance between sputtering and growth, and how the impact angles affect this. It was found that initial surface impacts caused the surface to roughen, exposing sub-surface layers and decreasing the average surface height. It was also found that when impacts had a polar angle of 50° to the surface normal or greater, surface erosion is the dominant factor dictating the surface evolution. This phenomenon has been indirectly suggested by other researchers who found that the sputter yield is greater than the atomic sticking probability in this same range of polar angle [41]. We have also found that the rate of surface erosion decreases at higher (>70°) polar angles, and again this aligns with previous MD simulation results [41].

The KMC simulation was developed with key processes designed to mimic those observed in the MD. These processes include surface sputtering and relaxation following the impact events. The processes were parameterised in terms of ranges and frequency, yielded many different combinations to explore in the KMC simulation phenomenology. Of these, the three most promising cases were chosen for quantitative comparison to the MD results for the same size of system. All three cases restricted surface relaxation to be close to the impact site, and included the Schwoebel barrier.

Of these, the best performing version was further utilised to study larger systems. It should be noted that even our best KMC version still showed some discrepancies in surface morphology when compared to the MD simulations, where the islands formed tended to be compact, suggesting that further improvements to the KMC methodology could be sought.

The KMC was deployed to study the evolution of the 56 × 28 surface model over long time scales. It was observed that this model suffered from finite size effects after the deposition of ~20 ML, indicating the limitations of MD simulations in terms of both lateral size and growth times. The KMC was readily deployed to explore larger systems for greater growth times, and it was found that the 56 × 56 and 112 × 56 surface models start to show finite size effects after the deposition of ~40 ML.

In conclusion, we have developed a KMC code that builds on MD results for surface evolution. The code captures the essential phenomena that are observed in the MD, allowing larger systems to be studied for longer growth times, permitting scrutiny of scaling and stepping towards a greater degree of predictability that is needed in the design of engineering scale processes.

There are wider implications of the work, since energetic atomic bombardment is an essential feature in many engineering scenarios such as thin film growth using plasma deposition and erosion in high-speed aeronautics. We have shown how the complexities revealed by the more realistic atomistic MD growth models can be captured in KMC growth rules, albeit in an ad hoc manner. To escalate the multiscale modelling approach further, continuum approaches could build upon these KMC rules to include surface relaxation and sputtering alongside deposition. It is clear that some care is needed to capture local versus nonlocal events, presenting interesting methodological challenges to further the development of simulation tools that are relevant to engineering applications.

Disclosure statement

No potential conflict of interest was reported by the author(s).

Data availability statement

Supplementary Material is available, describing the potential model used in the MD simulations.

ORCID

Andrew M. Bell 🔘 http://orcid.org/0000-0003-1656-1024
Paul A. Mulheran 🔘 http://orcid.org/0000-0002-9469-8010

References

[1] Orava J, Kohoutek T, Wagner T. Deposition techniques for chalcogenide thin films. In: J-L Adam, X Zhang, editors. Chalcogenide glasses: preparation, properties and applications. Cambridge: Woodhead Publishing; 2014. p. 265–309. doi:10.1533/9780857093561.1.265.

[2] Palharini RC, Scanlon TJ, White C. Chemically reacting hypersonic flows over 3D cavities: flowfield structure characterisation. Comput Fluids. 2018;165:173–187. doi:10.1016/j.compfluid.2018.01.029.

[3] Cong Z, Lee S. Study of mechanical behavior of BNNT-reinforced aluminum composites using molecular dynamics simulations. Compos Struct. 2018;194:80–86. doi:10.1016/j.compstruct.2018.03.103.

[4] Choi BK, Yoon GH, Lee S. Molecular dynamics studies of CNT-reinforced aluminum composites under uniaxial tensile loading. Compos B. 2016;91:119–125. doi:10.1016/j.compositesb.2015.12.031.

[5] Rezaei R, Shariati M, Tavakoli-Anbaran H, et al. Mechanical characteristics of CNT-reinforced metallic glass nanocomposites by molecular dynamics simulations. Comput Mater Sci. 2016;119:19–26. doi:10.1016/j.commatsci.2016.03.036.

[6] Dikshit MK, Engle PE. Investigation of mechanical properties of CNT reinforced epoxy nanocomposite: a molecular dynamic simulations. Mater Phys Mech. 2018;137:7–15. doi:10.18720/MPM.3712018_2.

[7] Tang D-M, Ren C-L, Wei X, et al. Mechanical properties of bamboo-like boron nitride nanotubes by in situ TEM and MDSimulations: strengthening effect of interlocked joint interfaces. ACS Nano. 2011;5:7362–7368. doi:10.1021/nn202283a.

[8] van der Walt C, Terblans JJ, Swart HC. Temperature- and surface orientation-dependent calculated vacancy formation energy for Cu nanocubes. J Mater Sci. 2018;53:814–823. doi:10.1007/s10853-017-1502-y.

[9] Doye JPK, Wales DJ. Global minima for transition metal clusters described by Sutton-Chen potentials. New J Chem. 1998;22:733–744. doi:10.1039/A709249K.

[10] Rafii-Tabar H, Shodja HM, Darabi M, et al. Molecular dynamics simulation of crack propagation in fcc materials containing clusters of impurities. Mech Mater. 2006;38:243–252. doi:10.1016/j.mechmat.2005.06.006.

[11] Mahboobi SH, Meghdari A, Jalili N, et al. (2008). Planar molecular dynamics simulation of metallic nanoparticles manipulatio. IEEE, 2008 8th IEEE Conference on Nanotechnology, Arlington, TX, USA. 163–166. doi:10.1109/NANO.2008.55.

[12] Khoei AR, Qomi MJA, Kazemi MT, et al. An investigation on the validity of Cauchy–Born hypothesis using Sutton-Chen many-body potential. Comput Mater Sci. 2009;44:999–1006. doi:10.1016/j.commatsci.2008.07.022.

[13] Tersoff J. New empirical approach for the structure and energy of covalent systems. Phys Rev B. 1988;37:6991–7000. doi:10.1103/PhysRevA.8.1504.

[14] Finnis MW, Sinclair JE. A simple empirical N-body potential for transition metals. Philos Mag A. 1984;50:45–55. doi:10.1080/01418618408244210.

[15] Sutton AP, Chen J. Long-range Finnis-Sinclair potentials. Philos Mag Lett. 1990;61:139–146. doi:10.1080/09500839008206493.

[16] Rafii-Tabar H, Sutton AP. Long-range Finnis-Sinclair potentials for f.c.c metallic alloys. Philos Mag Lett. 1991;63:217–224. doi:10.1080/09500839108205994.

[17] Joe M, Moon MW, Oh J, et al. Molecular dynamics simulation study of the growth of a rough amorphous carbon film by the grazing incidence of energetic carbon atoms. Carbon. 2012;50:404–410. doi:10.1016/j.carbon.2011.08.053.

[18] Hansen U, Vogl P, Fiorentini V. Atomistic modeling of large-scale metal film growth fronts. Phys Rev B. 1999;59:R7856–R7859. doi:10.1103/PhysRevB.59.R7856.

[19] Hansen U, Rodgers S, Jensen KF. Modeling of metal thin film growth: linking angstrom-scale molecular dynamics results to micron-scale film topographies. Phys Rev B. 2000;62:2869–2878. doi:10.1103/PhysRevB.62.2869.

[20] Buldum A, Busuladzic I, Clemons CB, et al. Multiscale modeling, simulations, and experiments of coating growth on nanofibers. Part I. Sputtering. J Appl Phys. 2005;98:044303. doi:10.1063/1.2007848.

[21] Buldum A, Clemons CB, Dill LH, et al. Multiscale modeling, simulations, and experiments of coating growth on nanofibers. Part II. Deposition. J Appl Phys. 2005;98:044304. doi:10.1063/1.2007849.

[22] Hansen U, Kersch A. Reaction rates for ionized physical vapor deposition modeling from molecular-dynamics calculations: effect of surface roughness. Phys Rev B. 1999;60(14):14417–14421. doi:10.1103/PhysRevB.60.14417.

[23] Vogl P, Hansen U, Fiorentini V. Multiscale approaches for metal thin film growth. Comput Mater Sci. 2002;24:58–65. doi:10.1016/S0927-0256(02)00164-7.

[24] Abrams CF, Graves DB. Three-dimensional spatiokinetic distributions of sputtered and scattered products of Ar+ and Cu+ impacts onto the Cu surface: molecular dynamics simulations. IEEE Trans Plasma Sci. 1999;27:1426–1432. DOI: 10.1109/27.799821.

[25] Abrams CF, Graves DB. Cu sputtering and deposition by off-normal, near-threshold Cu+ bombardment: Molecular dynamics simulations. J Appl Phy. 1999;86:2263–2267. DOI: 10.1063/1.371040.

[26] Coronell DG, Hansen DE, Voter AF, et al. Molecular dynamics-based ion-surface interaction models for ionized physical vapor deposition feature scale simulations. Appl Phys Lett. 1998;73:3860–3862. doi:10.1063/1.122917.

[27] Ahn H-S, Kim T-E, Cho E, et al. Molecular dynamics study on low-energy sputtering properties of MgO surfaces. J Appl Phys. 2008;103:073518. doi:10.1063/1.2899182.

[28] El Marsi M, Moultif R, Lahlou S, et al. Monte Carlo simulations of MgO and Mg(OH)2 thin films sputtering yields by noble-gas ion bombardment in plasma display panel PDP. Nucl Instrum Methods Phys Res Sect B Beam Interact Mater Atoms. 2018;430:72–78. doi:10.1016/j.nimb.2018.05.046.

[29] Ho S, Tamakoshi T, Ikeda M, et al. Net sputtering rate due to hot ions in a Ne-Xe discharge gas bombarding an MgO layer. J Appl Phys. 2011;109:084908. doi:10.1063/1.3554687.

[30] Henkelman G, Jónsson H. Long time scale kinetic Monte Carlo simulations without lattice approximation and predefined event table. J Chem Phy. 2001;115:9657–9666. doi:10.1063/1.1415500.

[31] Zhou Y, Lloyd AL, Smith R, et al. Modelling thin film growth in the Ag–Ti system. Surf Sci. 2019;679:154–162. doi:10.1016/j.susc.2018.08.020.

[32] Scott C, Blackwell S, Vernon L, et al. Atomistic surface erosion and thin film growth modelled over realistic time scales. J Chem Phys. 2011;135:174706. doi:10.1063/1.3657436.

[33] Jónsson H. Theoretical studies of atomic-scale processes relevant to crystal growth. Ann Rev Phys Chem. 2000;51:623–653. doi:10.1146/annurev.physchem.51.1.623.

[34] Swope WC, Andersen HC, Berens PH, et al. A computer simulation method for the calculation of equilibrium constants for the formation of physical clusters of molecules: application to small water clusters. J Chem Phys. 1982;76:637–649. doi:10.1063/1.442716.

[35] Toxvaerd S, Dyre JC. Communication: shifted forces in molecular dynamics. J Chem Phys. 2011;134:081102. DOI: 10.1063/1.3558787.

[36] Hockney RW, Eastwood JW. Computer simulation using particles. New York: McGraw-Hill; 1981; ISBN-13: 978-0070291089.

[37] Quentrec B, Brot C. New method for searching for neighbors in molecular dynamics computations. J Comput Phys. 1973;13:430–432. DOI: 10.1016/0021-9991(73)90046-6.

[38] Berendsen HJC, Postma JPM, van Gunsteren WF, et al. Molecular dynamics with coupling to an external bath. J Chem Phys. 1984;81:3684–3690. doi:10.1063/1.448118.

[39] Bell AM. (2019). Multi-scale material growth and erosion in extreme environments [PhD thesis]. University of Strathclyde. DOI: 10.48730/mgr2-y156.

[40] Barabási A-L, Stanley HE. Linear theory. In: Fractal concepts in surface growth. Cambridge: Cambridge University Press; 1995. p. 44–55. doi:10.1017/CBO9780511599798.

[41] Hanson DE, Stephens BC, Saravanan C, et al. Molecular dynamics simulations of ion self-sputtering of Ni and Al surfaces. J Vacuum Sci Technol A. 2001;19:820–825. doi:10.1116/1.1365134.